# The retinoid agonist Tazarotene promotes angiogenesis and wound healing

Accepted Article Preview: Published ahead of advance online publication


# The retinoid agonist Tazarotene promotes angiogenesis and wound healing

Ayman Al Haj Zen, Dorota A Navarro, Alison Howarth, Andrea Caporali, Daniel Ebner, Aude Vernet, Jurgen E Schneider, Shoumo Bhattacharya

**Cite this article as:** Ayman Al Haj Zen, Dorota A Navarro, Alison Howarth, Andrea Caporali, Daniel Ebner, Aude Vernet, Jurgen E Schneider, Shoumo Bhattacharya, The retinoid agonist Tazarotene promotes angiogenesis and wound healing, *Molecular Therapy* accepted article preview online 02 August 2016; doi:10.1038/mt.2016.153





Received 03 February 2016 ; accepted 26 July 2016 ; Accepted article preview online 02 August 2016

# The retinoid agonist Tazarotene promotes angiogenesis and wound healing

Ayman Al Haj Zen [1,2,#], Dorota A Nawrot[1], Alison Howarth[3], Andrea Caporali[4], Daniel Ebner[3], Aude Vernet[1], Jurgen E Schneider[1], Shoumo Bhattacharya[1]

[1] Wellcome Trust Centre For Human Genetics, Division of Cardiovascular Medicine, Radcliffe Department of Medicine, University of Oxford, Oxford, UK

[2] British Heart Foundation Centre of Research Excellence, University of Oxford, Oxford, UK

[3] Target Discovery Institute, Nuffield Department of Medicine, University of Oxford, Oxford, UK

[4] University/BHF Centre for Cardiovascular Science University of Edinburgh, Edinburgh, UK



**Running title:** Tazarotene promotes angiogenesis

**# Correspondence:**

**Ayman Al Haj Zen, MD, PhD**

Wellcome Trust Centre For Human Genetics

Division of Cardiovascular Medicine

University of Oxford

Roosevelt Drive

OX3 7BN Oxford

United Kingdom

**Tel: +44 1865 287 769**

**Email:** aymanzen@well.ox.ac.uk

**Abstract**

Therapeutic angiogenesis is a major goal of regenerative medicine, but no clinically approved small molecule exists that enhances new blood vessel formation. Here we show, using a phenotype-driven high-content imaging screen of an annotated chemical library of 1280 bioactive small molecules, that the retinoid agonist Tazarotene, enhances *in vitro* angiogenesis, promoting branching morphogenesis, and tubule remodeling. The pro-angiogenic phenotype is mediated by Retinoic Acid Receptor (RAR) but not Retinoic X Receptor (RXR) activation, and is characterized by secretion of the pro-angiogenic factors Hepatocyte Growth Factor (HGF), Vascular Endothelial Growth Factor (VEGFA), Plasminogen Activator, Urokinase (PLAU) and Placental Growth Factor (PGF), and reduced secretion of the anti-angiogenic factor Pentraxin-3 (PTX3) from adjacent fibroblasts. *In vivo*, Tazarotene enhanced the growth of mature and functional microvessels in Matrigel implants and wound healing models, and increased blood flow. Notably, in ear punch wound healing model, Tazarotene promoted tissue repair characterized by rapid ear punch closure with normal-appearing skin containing new hair follicles, and maturing collagen fibers. Our study suggests that Tazarotene, an FDA-approved small molecule, could be potentially exploited for therapeutic applications in neovascularization and wound healing.



**Keywords:** High content screening, Tazarotene, Retinoic acid, Endothelial cell, Angiogenesis, Wound healing

## Introduction

Angiogenesis, the growth of new vessels from pre-existing ones, plays a critical role in tissue renewal and repair. Insufficient angiogenic response occurs in diseases, such as ischemic heart disease, peripheral arterial disease, Alzheimer's disease, ulcers, and chronic wound healing causing dysfunction of repair and regeneration[1-3]. Currently no clinically approved small molecule exists that enhances new blood vessel formation. Clinical efforts to develop pro-angiogenic therapies have largely focused on administration of single pro-angiogenic growth factors such as VEGF and FGF using recombinant protein or gene transfer technologies[4,5], but these are currently viewed as being only modestly successful[6], possibly because therapeutically beneficial levels of growth factors are not achieved[7], or that the cooperative molecular interactions necessary for the establishment of a functional vascular network are not achieved through a single growth factor[8], or indeed that such complex molecular interactions and therapeutic targets are only partially understood.

Phenotype-driven approaches can overcome this knowledge gap by minimizing assumptions regarding molecular interactions and targets and instead focusing directly on functional aspects of vascular network formation[9]. The unbiased identification of therapeutically active molecules using direct phenotypic screens is now possible using high-content microscopy and image analysis algorithms to generate quantitative phenotypic data[10]. Provided an appropriate *in vitro* model of *in vivo* angiogenesis is used, such phenotype-driven screens could identify pro-angiogenic molecules that could be therapeutically translated.

The growth of new functional blood vessel network is determined by the extent of branching and tubulogenesis. The endothelial tube formation assay recapitulates most cellular process involves in the assembly of endothelial cells into a primary plexus (e.g. cell-cell, cell-matrix interaction) and has a high predictive value for angiogenesis-related cellular morphogenesis such as vascular branching and, suggesting that this is an appropriate model for *in vivo* angiogenesis[11,12]. We developed a high content imaging approach using the endothelial tube formation assay to screen small molecule libraries with aim

of identifying novel therapeutic molecules that enhance new blood vessel growth. Here, we identify and characterize Tazarotene, a small molecule that promotes endothelial tubulogenesis and branching. We also demonstrate that systemic delivery of Tazarotene stimulates functional neovascularization and accelerates wound healing.

## Results

### High content screen of small molecule library using endothelial tube formation assay

The endothelial tube formation assay is quantifiable, rapid, and reproducible, and measures key features of angiogenesis such as branching and tubulogenesis[13 14]. We miniaturized the assay to a 384-well plate format, and established a Z' factor (a statistical measure of assay robustness) for total tube length of 0.33, which is acceptable for high-throughput cell-based screening **(Supplementary Fig. 1)**. To identify small molecules capable of enhancing endothelial tube formation, we screened a Library Of 1280 Pharmacologically Active Compounds (LOPAC) in a 384-well plate format at a final compound concentration of 10 μM. Primary screening of the LOPAC library included four 384-well plates with a Z' factor of 0.48 ±0.13 and a hit rate of 1.1% for tube formation enhancers and 6.2% for inhibitors **(Supplementary Fig. 2a, Fig. 1)**. As branching points and total tube length were positively correlated **(Supplementary Fig. 2b)**, we used total tube length as the parameter for hit selection, using a B-score threshold >+2.6 and <-4 for identifying enhancers and inhibitors respectively. The screen resulted in an initial active compound list of 79 inhibitors and 15 enhancers **(Supplementary Table 1 & 2)**. One enhancer hit was excluded from the list after visual examination of the well images because of a technical artifact. We re-assayed the 14 enhancers using three independent five-point dose dependence trials (1.25 μM to 20 μM) in 96-well plates using the same image analysis algorithm used in the primary screen. Three compounds increased significantly and consistently the total tube length by more that 15% over the negative control **(Fig. 2a)**. To re-confirm the results of the screen, we re-examined three active lead compounds in an independent organotypic assay for angiogenesis, in which fibroblasts were co-

cultured with endothelial cells (**Fig. 2b**). We found that the dopamine re-uptake inhibitor (GBR-12909) reduced tubulogenesis and branching whereas the P38 kinase inhibitor (SB202190) modestly increased the tubulogenesis and branching. The retinoid agonist Tazarotene showed a robust pro-angiogenic activity reflected by around 60% increase in total tube length and branching points compared to controls, and was therefore followed-up further.

**Tazarotene promotes endothelial tube remodeling and branching**

Tazarotene is a synthetic third generation retinoid that is approved by the US Food and Drug Administration for the topical treatment of plaque psoriasis and acne vulgaris[15]. We measured the $EC_{50}$ of Tazarotene (concentration required to enhance the total tube length by 50%) in the organotypic angiogenesis assay. The $EC_{50}$ of Tazarotene (800 nM) in this assay is comparable to the $EC_{50}$ of other retinoids in cell-based phenotypic assays[16], suggesting that enhancement of endothelial tube formation was unlikely to be an off-target effect **(Fig. 2c)**. We observed a distinctive pattern of the organotypic vascular-like network after treatment of Tazarotene, characterized by highly branched, thinner tubes, minimal cell clustering, and increased filopodia formation in the lateral sides of outgrowing endothelial tubes **(Fig. 2d)**. The increase in branching triggered by Tazarotene was noted from 3 days following endothelial cell seeding onto fibroblasts (the early phase of network formation) **(Supplementary Fig. 3a)**. To evaluate the behavior of the newly forming endothelial tubes following Tazarotene treatment, we traced GFP-expressing HUVECs in co-culture by live cell imaging in the initial phase of network formation. Control endothelial cells initially form clusters with minimal remodeling and branch formation at this stage **(Supplementary Fig. 3b)**. In contrast, with Tazarotene treatment, endothelial cells elongated and sprouted, and endothelial tubes remodeled more rapidly than controls, becoming thinner with time **(Supplementary Fig. 3b)**. However, Tazarotene did not affect endothelial cell motility in single cell culture or in co-culture measured over 24 hours **(Supplementary Fig. 4)**. VEGFR2 & VEGFR3 expression is very low or absent in most adult blood vessels, but expression is up-

regulated in angiogenic endothelial cells and in endothelial tip cells[17,18]. We therefore investigated VEGFR2 & VEGFR3 expression in cultured endothelial cells after Tazarotene treatment, and found that it augmented VEGFR3 but not VEGFR2 expression **(Fig 2e)**. Taken together, these findings show that Tazarotene induces sprouting behavior of endothelial cells and tubule remodeling.

**Tazarotene promotes angiogenesis via retinoic acid receptor activation**

The biologically active form tazarotenic acid is produced by esterase hydrolysis of tazarotene in the skin, and binds to three members of the RAR family of retinoid nuclear receptors, with relatively more selectivity for RARβ and RARγ[19]. We therefore investigated whether the observed pro-angiogenic effect of tazarotene is mediated via retinoic acid signaling. We used a pharmacological rather than a genetic approach here as combinatorial isoform specific siRNA for the many retinoid receptor isoforms is technically challenging. To quantify angiogenesis in the experiment set, we measured multiple parameters depicting the vascular-like network in the organotypic angiogenesis assay after different treatments. We then hierarchically clustered the compounds into distinct angiogenic phenotypes based on four angiogenic parameters: total tube length, branching points, tube thickness and total node area. All-*trans*-retinoic-acid (ATRA) exhibited the most similar pro-angiogenic phenotype to Tazarotene, suggesting that effects are via the canonical pathway **(Fig. 3a)**. Similar effects were observed using 9-*cis*-retinoic acid, which is an intracellular product of ATRA isomerization, confirming the effects of Tazarotene through activation of RAR **(Fig. 3a)**. While the selective pan RXR agonist (SR 11237) slightly increased total tube length and branching, endothelial tubes were thicker with greater cell clustering (nodes), unlike the Tazarotene- or ATRA-induced phenotypes **(Fig. 3a)**. We next examined the effect of isoform selective RAR agonists[20,21]. We found that selectvie RARβ or RARγ agonists (CD2314 and BMS961 respectively) reproduced the distinct pro-angiogenic phenotype of Tazarotene. The selective RARα agonist (BMS 753) increased overall tube formation to a lesser extent than RARβ or RARγ agonists **(Fig. 3a)**. As a complementary approach, we also examined the effect of RAR and

RXR blockade on Tazarotene-induced angiogenesis. The addition of the pan-retinoic acid receptor inverse agonist (BMS493) attenuated the ability of Tazarotene to enhance the angiogenesis. In contrast, the incubation of Tazarotene with an RXR antagonist (UVI3003)[22] did not affect the pro-angiogenic phenotype of Tazarotene **(Fig. 3b)**. These data clearly indicate that the effect of Tazarotene on the branching tubule remodeling is only mediated through RAR binding. We next investigated the effect of Liarozole, a retinoic acid metabolic blocking agent that inhibits the cytochrome P450 (CYP26A1)-dependent catabolism of retinoic acid, thereby increasing intracellular retinoic acid[23]. Liarozole treatment induced the tube formation and increased endothelial branching compared to controls **(Fig. 3c)**. We next examined the expression of RARRES1, a specific downstream target gene for retinoic signaling activation[24]. Tazarotene induced RARRES1 mRNA expression 6-fold in endothelial cells and 40-fold in fibroblasts **(Fig. 3d)**. Taken together these data indicate that the pro-angiogenic effect of Tazarotene is through the canonical retinoic acid-signaling pathway via RAR and not RXR activation.



**Tazarotene enhances the pro-angiogenic paracrine effects of fibroblasts**

Given the known link between cell growth and angiogenesis, we next evaluated cell proliferation following Tazarotene treatment. When endothelial cells were cultured alone, their cell numbers (as measured by DAPI) were decreased slightly after treatment with Tazarotene doses up to 10 μfgM but the decrease was more pronounced at 20 μM. The level of DNA synthesis (as measured by EdU incorporation) did not change significantly **(Fig. 4a)**. In the organotypic angiogenesis co-culture experiments, endothelial cells were stained with anti-CD31 antibody and subsequently the total cell number and percentage of EdU-positive cells were quantified in both endothelial cells ($CD31^+$) and fibroblasts ($CD31^-$). We found that Tazarotene treatment did not affect either endothelial or fibroblast cell numbers significantly, at doses up to 10 μM, but reduced fibroblast cell numbers at 20 μM. We also observed an increase in DNA synthesis of fibroblasts at doses from 1-10 μM **(Fig. 4b)**. Thus there does

not appear to be a significant effect of Tazarotene on endothelial cell number or DNA synthesis when they are co-cultured with fibroblasts.

As retinoic acid can induce vascular growth factors such as VEGF and HGF[25,26], we next explored the effect of Tazarotene on the secretion of angiogenesis-related factors profile from fibroblasts. Using a comparative proteome profiler array of 55 different cytokines we found that Tazarotene increased the secretion of the vascular growth factors VEGFA, HGF, PGF and PLAU[27]) whereas the secretion of PTX3, an inhibitor of angiogenesis[28] was decreased **(Fig. 4c)**. We found that Tazarotene up regulated PGF mRNA expression, whereas PTX3 mRNA expression was decreased **(Fig. 4d)**. Furthermore, we validated the enhanced secretion of PGF and PTX3 by ELISA **(Fig. 4e)**. These data suggest that the pro-angiogenic effect of Tazarotene is more pronounced in the co-culture angiogenesis model partly because of paracrine effects, which amplify the angiogenic response.



**Tazarotene stimulates *in vivo* functional neovascularization**

To investigate whether systemically administered Tazarotene enhanced *in vivo* neovascularization, we tested its efficacy in Matrigel implants implanted in mice. Intra-peritoneal administration of Tazarotene was well tolerated **(Supplementary Fig. 5)** and resulted in enhanced expression of hepatic RARRES1 (a retinoid pathway target[22]) indicating that Tazarotene was systemically bioactive **(Supplementary Fig. 6)**. The invasion and the growth of microvessels into the Matrigel implant was quantified by CD31 and □-smooth muscle (SM) actin staining of endothelium and mural cells, and was significantly higher following systemic Tazarotene. Moreover, the neovessels formed appeared more mature and covered by mural cells (α-SM actin positive cells) **(Fig. 5b)**. We quantified neovessel perfusion by perfusing mice with Microfil, and imaged dissected plugs using microCT. Microvessels penetrating the Matrigel implant are more abundant in the Tazarotene treated group (7-folds *versus* control) and invading neovessels penetrate deeper into the gel **(Fig. 5c)**. To visualize the structure and perfusion of microvasculature at a cellular level, we perfused mice with biotinylated-isolectinB4. Thick section

preparations of Matrigel revealed that Tazarotene increased the formation of microvessels with an enhanced capacity to receive flow whereas fewer microvessels could be identified in control mice **(Fig. 5d)**.

**Tazarotene enhances wound vascularization and healing**

Angiogenesis is a critical part of the normal healing process. New blood vessels deliver oxygen, nutrients, and essential growth factors to injured tissues[29]. To assess its effect on wound angiogenesis, first we used an ear punch wound model. The ear punch model is an established model of wound healing model and has been widely used to study wound healing, tissue regeneration, innervation and neovascularization [30, 31, 32, 33]. In particular, quantitative analysis of new vessel formation and wound morphometry is feasible in this model. Tazarotene was injected intraperitoneallly for six days following injury. The group treated with Tazarotene showed a remarkable acceleration of wound closure measured after 12 days **(Fig. 6a)**. Blood flow and tissue perfusion was measured by contrast speckle laser imaging at 6 and 12 days following injury and was significantly enhanced in the regenerating area of the Tazarotene-treated group **(Fig. 6b)**. Histologically, a major difference in ear hole size with neogenesis of hair follicles **(Fig. 6c, Supplementary Fig. 7)** was apparent at the wound margins by day 14 after Tazarotene. The re-differentiation events such as hair follicle growth are considered later morphogenetic events in the regenerative healing process[34]. Collagen is a major extracellular matrix component of skin and essential for the mechanical properties of the wounded region. We assessed the collagen fiber networks using staining with picrosirius red (a dye for collagen fiber maturity[35]). The new and mature collagen levels were increased in the regenerated area in the Tazarotene-treated group compared to the control group. Collagen fiber morphology and organization was close to that observed in the normal skin in the Tazarotene treated group **(Fig. 6c)**. Proliferating cells were more abundant in regenerating area of the Tazarotene-treated group. The majority of the proliferating cells were epithelial (K14 positive) cells). Fewer proliferating cells were detected in the vessels or myofibroblasts (α-smooth muscle cell positive

cells) **(Fig. 6d)**. Blood vessel densities in the regenerated ear margin of Tazarotene-treated mice were 4.5-folds greater than that seen in Vehicle-treated mice **(Fig. 6e)**. Confocal microscopy of ear whole mount revealed an augmented neovessel growth in the regenerated tissue of the Tazarotene-treated group at 14 days after injury. Notable, a significant increase of sprouting vessels towards the wound edge is detected as early as 4 days after injury **(Fig 6f,g)**. The ear punch model provides cartilage as the wound bed. To further explore the therapeutic potential of Tazarotene in a model that does not involve cartilage, we have used a dermal excisional wound model. In agreement with our previous findings in the ear punch wound model, we found that animals treated with Tazarotene showed an acceleration of wound healing (**Fig 7a**). Histological analysis revealed that Tazarotene increased wound epithelialization (**Fig 7b**) and enhanced new microvessel growth (**Fig 7c**) in the wound bed compared to the control group. Together, these data show that Tazarotene induces wound tissue repair associated with increased neovascularization of the wound bed.



**Discussion**

In the present study, we used high content imaging techniques and a combination of two phenotypic angiogenesis assays to screen a small molecule library with well-defined targets. This resulted in the identification of Tazarotene, a third generation retinoid agonist, as a pro-angiogenic small molecule. We showed that Tazarotene promotes blood vessel growth and functional neovascularization in several *in vitro* and *in vivo* systems that model angiogenesis.

At a cellular level, we show that Tazarotene increases the generation of endothelial cell filopodial protrusions and tubule remodeling, resulting in a highly branched vascular network. The vascular network can be grown through elongation or branching of adjacent endothelial cells. When endothelial cells are seeded onto fibroblasts, they initially form clusters, which remodel later and sprout to form a vascular-like network[36]. Notably, Tazarotene predominantly accelerates this process of remodeling, by enhancing the differentiation of endothelial cells towards an elongated phenotype with increased

filopodia formation. Confirming this, Tazarotene enhances VEGFR3 transcription in endothelial cells. Importantly, VEGFR3 is increased in sprouting endothelial cells during the growth of new vessels[17], and blockade of VEGFR3 signaling results in decreased sprouting, vascular density, vessel branching and endothelial cell proliferation[37]. By following tubule formation in co-cultures by time-lapse microscopy, it appears that Tazarotene enhances tubule remodeling rather than cell migration.

Retinoids act via RARs and RXRs, nuclear transcription factors, which form homo and heterodimers that bind the enhancers of retinoid-responsive genes[38]. Using a pharmacological approach, we showed that the angiogenic phenotype induced by Tazarotene is dependent on the specific activation of RARs but not RXRs. The resemblance of the RARβ and RARγ dependent pro-angiogenic phenotypes *in vitro* is consistent with the binding of the active form of Tazarotene to all three RARs with increased selectivity for RARβ and RARγ, The induction of RARRES1 – a gene that is up regulated by RAR but not RXR specific synthetic retinoids[24] – by Tazarotene in both endothelial cells and fibroblasts also supports the idea that RARs are instrumental in driving the Tazarotene-generated angiogenic phenotype. This is a novel supporting evidence that Retinoic acid can have angiogenesis-promoting activity [39].

We showed that blockade of retinoic acid degradation, which leads to increase the intracellular level of retinoic acid, induces the sprouting angiogenic behavior of endothelial cells similar to Tazarotene. The intracellular level of retinoic acid is maintained by the balance between its synthesis and degradation into inactive products, and is regulated by an enzymatic network in which retinol dehydrogenases (RDH) and retinaldehyde dehydrogenases (RALDHs) synthesize, while cytochrome the P450 CYP26 degrades retinoic acid[40]. This generates gradients of retinoic acid signaling activity that are distributed in a dynamic spatiotemporal manner to create important control mechanisms during organ development[41,42]. We speculate that such gradients may similarly program the sprouting and remodeling process during new vessel formation. The regulation of intracellular retinoic acid availability could thus be an important factor in controlling the different cellular events of angiogenesis.

In our study, an important observation is that the pro-angiogenic effect of Tazarotene is magnified when endothelial cells are co-cultured with fibroblasts, suggesting a role for paracrine secretions from fibroblasts in mediating this effect. We observed around 60% enhancement of tube formation when Tazarotene was added to endothelial cell/fibroblast co-culture. This is in contrast to around 18% enhancement of tube formation when Tazarotene was applied to endothelial cell culture. Consistent with this, we demonstrate that Tazarotene induces the secretion of the pro-angiogenic factors VEGFA, HGF, PGF[43] and PLAU from fibroblasts. Moreover, Tazarotene decreases the secretion of PTX3, an inhibitor of angiogenesis [44].

Our results indicate that in endothelial cell/fibroblast co-culture, Tazarotene enhances human fibroblast DNA synthesis. However Ogawa et al [45] reported a reduction in fibroblast DNA synthesis with Tazarotene when cultured in isolation. We speculate that this difference may be due to the experimental conditions, the most important being that we used a co-culture with endothelial cells.

The pro-angiogenic properties of Tazarotene, identified in our cell-based studies, were confirmed in relevant *in vivo* models – Matrigel implant and wound healing. In both models, angiogenesis is preceded by fibroblast growth and invasion. In the Matrigel plug model, we show that Tazarotene enhanced the formation of an anatomically mature neovessel network that was physiologically functional and able to receive blood flow. Moreover, we found that Tazarotene induced sprouting angiogenesis and capillary growth from an early stage of the healing process. Capillary growth into the wound allows delivery of nutrients, cells, and cytokines that mediate the healing response, and is necessary for metabolite removal. Insufficient angiogenesis thus impairs wound healing[46]. In our study, the induction of angiogenesis by Tazarotene was accompanied with histological signs of rapid repair in ear punch wounds as evidenced by increased regenerating tissue, establishment of organized mature collagen fiber network, increased proliferative activity in wound edges and hair follicle neogenesis. While retinoic acid can induce regeneration in a number of different organ systems in vertebrate such as the urodele amphibian limb [47], our data show that Tazarotene enhances both functional neovascularization and skin

tissue repair in adult mice, which are both essential components of the efficient repair process following injury.

In summary, we demonstrate that Tazarotene promotes neovascularization and tissue repair through its action on retinoic acid signaling. At least in part, this is driven by a Tazarotene-induced pro-angiogenic paracrine signaling from fibroblasts. Tazarotene is a small molecule with a defined mechanism of action, and is approved for topical use by the FDA[15]. Oral Tazarotene does not appear to be associated with adverse events that are typical of oral retinoids, including hypertriglyceridemia and hypercholesterolemia[48]. Thus, re-purposing of Tazarotene could be explored for treatment of pathological conditions where circulatory insufficiency is a significant factor, for instance in delayed wound healing [49].



## Materials and Methods

### Chemical compounds

The LOPAC[1280] library (Sigma) is a collection of 1280 pharmacologically active compounds from 56 pharmacological classes with well-characterized properties. Compounds were dissolved in DMSO and transferred to 384-well plates and stored at -20°C. Upon hit identification, all selected enhancer compounds including Tazarotene were purchased as powders from Sigma. All compounds were dissolved and aliquoted in DMSO at 10mM. RARα selective agonist (BMS753), selective RARβ agonist (CD2314), selective RARγ agonist (BMS961), RXR agonist (SR 11237), pan-RAR inverse agonist (BMS493), pan RXR antagonist (UVI30003) and Liarozole hydrochloride were purchased from TOCRIS. All-*trans*-Retinoic Acid and 9-*cis*-Retinoic Acid were purchased from Sigma.

**Development and miniaturization of endothelial tube formation assay for high throughput screenings**

Primary Human Umbilical Endothelial cells "HUVEC" were purchased from Lonza. Cells were maintained in endothelial cell Medium (EGM-2™, Lonza). Low passage cells (<5) were used for all experiments. The *in vitro* tube formation assay was performed as previously described for a 96-well microplate format[13]. In our study, we also adapted the assay for 384-well microplate format. Briefly, HUVEC were seeded at 15,000 cells per well for 96-well plate or 4,500 cells per well for 384-well plate on top of Matrigel (ref.354248, BD Bioscience) after adding compounds and incubated at 37°C, %5 $CO_2$ for eight hours. HUVEC formed capillary-like vascular structures "tubes" in the presence of the Matrigel. The tubes were fixed and stained with Alexa568-conjugated phalloidin (Invitrogen), HCS CellMask™ Green (Invitrogen) and DAPI (Invitrogen). Assays were performed in black-walled, clear-bottom, 96-well and 384-well microplates (Perkin Elmer) suitable for automated fluorescent imaging. Images were acquired using a high-content imaging system (Operetta, Perkin Elmer). The raw (.tiff) images were then segmented and analyzed to extract the morphological features of vascular-like network using fully-automated Metamorph image analysis software (Molecular Devices). The Z' factor was used to measure the robustness of the cell based assay. It is defined by the following equation:

$$Z' = 1 - \frac{3\,(SD_{pos\ control} + SD_{neg\ control})}{|mean_{pos\ control} - mean_{neg\ control}|}$$

Assays with Z>0.3 are considered highly suitable for conducting a high-throughput screening of assays with complex cellular systems such as capillary-like network formation[50]. We found that the most robust morphological parameter is total tube length (Z' factor=0.33). For the actual screen, several other parameters depicting the network morphometric were also measured including branching points, average tube thickness, total tube area, total node area, tube length per set and segment number.

**High content screening for regulators of angiogenesis**

Cooled Matrigel (16µl) was dispensed into black 384-well plates (F-bottomed, Cell carrier, Perkin Elmer) using liquid handling robotics (JANUS, Perkin Elmer) and incubated for one hour at 37°C. Next, library compounds (in 16µl media) were added to a final concentration of 10µM for further 30 min at room temperature. Suramin (inhibitor of angiogenesis)[44] was added as positive control and 0.5% DMSO (Vehicle) was added as negative control. HUVEC (pooled donor, C2519A, Lonza, passage 4) were grown in EGM™-2 Media (Lonza). Cells were split using Accutase® (Sigma). Cells were then seeded in the prepared plates with compounds and Matrigel at density of 4,500 cells per well in 16µfgl with cell dispenser (FlexDrop PLUS) and liquid handling robotics (JANUS). Microplates were incubated for eight hours at 37°C, %5 $CO_2$ until endothelial cells form capillary-like vascular structures "tubes". The screen was performed in duplicate.

Endothelial tubes were fixed with paraformaldehyde 4% overnight at 4°C. After washing with PBS, cells were permeabilised with 0.1% Triton X-100 in PBS for 10 min. Cells were stained with alexa fluor-568 phalliodin (Invitrogen), 1:200 and DCS CellMask™ Green (Invitrogen), 1:5000 for 45 min at room temperature. Wells were washed three times with 0.05% TWEEN-20 in PBS. Next, the plates were imaged with a 2x objective using a high-content microcopy system (Operetta, Perkin Elmer). A single field which covers the whole well was acquired at two wavelengths to image cell body (CellMask green) staining and actin phalloidin staining at exposure times of 50 and 400 milliseconds, respectively. The actin-phalloidin images (16-bit depth) were cropped using imageJ (NIH) to extract the region-of-interest from the row images and to remove the out-of-focus objects in the border area of the well. Each resulting well image had a dimension of 400x400 pixels, which covers 45% of the total area of the well. Next, the processed images were segmented and analyzed to extract the morphological features of the vascular-like network using fully-automated Metamorph image analysis software (Molecular Devices). A pixel intensity threshold was set to distinguish actin-labeled endothelial tubes from local background along with a minimum and maximum tube width and applied for analysis of all images.

The total tube length and branching points reading values were normalized using the B-score method in the WebCellHTS2 package[51]. The hit selection threshold was set at +2.6 for enhancers and at -4.0 for inhibitors. $R^2$ correlation between replicates was =0.7. The Z' factor was used to assess the quality control of the screen plates, and was >0.3 in all plates (**Supplementary Fig. 2a**). The screen data and plate QC assessment were visualized and analyzed using Excel (Microsoft), Spotfire (TIBCO, Perkin Elmer) and Prism (GraphPad) software.

**Co-culture angiogenesis assay**

Adult human dermal fibroblasts (HDF, Lonza) were seeded at density 15,000 cells per well. Next day, HUVEC were plated at density 4,000 cells per well on the confluent fibroblast monolayer in 96-well plate as described previously[52]. The interaction of these two cell types gives rise to three-dimensional tubules over a period of 5-7 days. The drug is added one hour after plating of HUVEC to avoid potential secondary effect of the drug on cell adhesion. The co-cultures were fed with a full-growth factor supplemented medium consisting of a 1:1 mixture of medium-106 (Invitrogen): EGM-2 medium. Endothelial formed tubes were assessed by immunofluorescence using a mouse anti-human CD31 monoclonal antibody (ref. BBA7, R&D systems) at 1:100 dilution and goat alexa 568-conjugated anti-mouse IgG secondary antibody (Invitrogen) at 1:400 dilution. Nuclei were visualized by DAPI staining. The endothelial tubes were imaged automatically at 10x magnification using the high-content imaging system (Operetta). Typically, nine identically positioned fields were acquired from each well in each experiment. Quantification of the angiogenic parameters of formed endothelial network was performed automatically using Metamorph software.

**Heat map clustering and analysis for phenotypic profiling of compounds**

Prior to hierarchical clustering, data were scaled by performing Z score normalization for each angiogenic parameter. Z score–transformed values were then clustered using an unsupervised

agglomerative clustering method with an average linkage and a Euclidian distance measurement[53]. Hierarchical clustering of the compound phenotype profiles was carried out using TIBCO Spotfire software and data were visualized using the dendrogram for compounds with heat map for angiogenic parameter values.

**Cell proliferation assay**

Cell proliferation was assessed using Click-iT® EdU Alexa Fluor® 488 HCS kit (ref. C10350, Invitrogen) according to the manufacturer's protocol. Briefly, HUVEC were seeded alone or on HDF monolayer in 96-well plates at $7.5\times10^3$ cells per well and treated with Tazarotene or Vehicle for 48 h. EdU labeling medium (10 μM final concentration) was added to the cell culture and incubated for 6 hours before fixation. Next, the cultured cells were fixed with 4% paraformaldehyde for 10 min and treated with 0.1% Triton X-100 for 15 min at room temperature. After washing with PBS, the samples were stained with Click-iT® reaction cocktail working solution at room temperature for 30 min. The cells were stained with DAPI at room temperature for 20 min. In co-culture experiments, endothelial cells were stained with mouse anti-human CD31 antibody (R&D systems) and subsequent incubation with alexa568-conjugated goat anti-mouse IgG secondary antibody (Invitrogen). The plates were imaged and quantified using high content fluorescent microscopy (Operetta). The total cell number and percentage of EdU-positive cells was calculated from 9 fields per well using a 10x objective (Harmony software, Perkin Elmer). The image analysis software (Harmony) has the required algorithms to be able to distinguish the nuclei in stained endothelial tubes from the ones of fibroblasts.

**Time-lapse live cell imaging and cell motility assessment**

HUVEC stably expressing eGFP were obtained by transduction of eGFP-puro-lentiviral vector (GeneCopoeia). HUVEC expressing eGFP were seeded in 96-well plate as single cells or were co-cultured with fibroblasts in presence of Tazarotene (7 μM) or Vehicle. Time-lapse live imaging was

performed in a humidified, heated and $CO_2$-controlled and integrated chamber within the high-content imaging system (Operetta). For cell motility assessments, images were captured with 10x objective at 15 min intervals for a total period of 24 hours. Individual cells were identified and tracked automatically within the field image using Harmony image analysis software. For observing tubulogenesis, images were captured with 10x objective at 15 min interval for a total period of 48 hours.

**Proteome profiler array for angiogenic factors**

The Proteome Profiler Human angiogenesis-related cytokines Array Kit (R&D Systems, Catalog # ARY007) was used to analyze secretory changes in the conditioned medium of fibroblasts following Tazarotene or Vehicle treatments for 48 hours essentially according to the manufacturer's instructions, but using IRDye® 800CW streptavidin. Visualization and quantitation of the detected spots were performed using the LI-COR Odyssey scanner and Odyssey 3.0 analytical software (LI-COR Biosciences). Pixel density values in dot blots were corrected by normalizing to the highest average control and subtracting the average pixel density values of negative controls. The map array of cytokines is illustrated in (supplementary Fig. 5).



**Quantitative RT-PCR**

Total RNA was isolated from cultured cells using the Qiagen RNeasy Micro Kit and from the mouse liver using the Qiagen RNeasy Mini Kit according to the manufacturer's protocol. cDNA was prepared with QuantiTect Reverse Transcription Kit (Qiagen). SYBR green qPCR was carried out with the following QuantiTect Primer Assay assays: Human FLT4, Hs_FLT4_1_SG (QT00063637), Human KDR, Hs_KDR_1_SG (QT00069818), Human RARRES1, Hs_RARRES1_2_SG, (QT01666469) Human PGF, Hs_PGF_1_SG (QT00030688), Human PTX3, Hs_PTX3_1_SG (QT00093261) and mouse RARRES1, Hs_RARRES1_2_SG, (QT01666469) . The data were normalized to the endogenous controls HPRT1, Hs_HPRT1_1_SG, (QT00059066) for cells and 18S ribosomal RNA,

Mm_Rn18s_3_SG, (QT02448075) for murine samples. Fold changes were calculated using comparative ddCT (threshold cycle) method (BioRad).

**ELISA**

We used commercially available enzyme-linked immunosorbent assay (ELISA) kits (DuoSet, R&D systems) to measure thuman Placental Growth factor (PGF) and Pentatraxin 3 (PTX3) levels in cell culture supernatants.

***In vivo* Matrigel implant angiogenesis assay**

Experiments involving mice were covered by project and personal licenses issued by the UK Home Office and they were performed in accordance with the Guide for the Care and Use of Laboratory Animals (the Institute of Laboratory Animal Resources, 1996). Eight-week old female CD1 mice (Harlan Laboratories) were injected subcutaneously into both abdominal flanks with 400µl growth factor-reduced Matrigel (BD Bioscience) supplemented with FGF2 (250ng/ml, R&D systems), under anesthesia induced by isoflurane inhalation. Mice were daily injected intra-peritoneally (i.p.) with either Tazarotene (10mg/kg) or 2.5% DMSO in PBS (Vehicle) starting from the day of Matrigel implantation for 6 days. Twelve days later, the mice were killed and Matrigel implants were removed, photographed and fixed in 4% paraformaldehyde at 4°C overnight. Implant paraffin sections of 7µm thickness were incubated with the rat anti-mouse CD31 antibody (1:100, BD Biosciences, 550274) overnight at 4ºC. Sections were then incubated with alexa488 conjugated goat anti-rat IgG secondary antibody (Invitrogen) and cy3-conjugated anti–α-smooth muscle actin antibody (Sigma). Nuclei were counterstained with DAPI. Mounted sections were imaged with 20x objective by Operetta imaging system (Perkin Elmer). Microvessel density was quantified in 30-40 fields covering the whole cross-section of the Matrigel plug at each of three 1-mm spaced sectioning planes of implants. CD31 positive

neovessel area covered with α-smooth muscle actin positive cells inside implants and total implant area were quantified using Image J software (NIH).

To visualize microvessel perfusion, terminally anesthetized mice were injected intracardially with 3mg/kg of biotinylated GS-IsolectinB4 (invitrogen). After 5 min, mice were euthanized and perfused with 4% neutral buffered paraformaldyhede under physiological pressure. Implants were dissected and stored in PFA 4% overnight. Following an incubation in 30% (w/v) sucrose solution, the plugs were embedded in OCT compound and were snap frozen. Implants were cut into thick sections (200μm) and labeled for injected lectin by incubating with alexa647-conjugated streptavidin. Co-staining is applied to visualize the total vessels by incubating with anti-CD31 antibody as described above. Fluorescence images of stained slices were taken with a confocal laser-scanning microscope (Zeiss 510 Metahead). Around 50 *z*-stacks of raw images (*xy*) were required for 3D reconstruction.



**MicroCT angiogram**

Mice were euthanized, and the thoracic cavity was opened. The right atrium was cut, and the heart (left ventricular) flushed with PBS containing heparin (1000 IU/L) for 5 min. 4% neutral buffered paraformaldyhede was perfused under physiological pressure for an additional 5 min. A contrast agent, radiopaque silicone rubber compound (Microfil, MV-112, Flow Tech Inc.), was injected into the heart for 5 min as described previously[54]. Obvious perfusion in the eyes and tail served as a reliable marker for systemic perfusion of the blood circulation. The mice were left at room temperature for 30 min to allow polymerization of the agent. Matrigel implants including the overlying skin were generously dissected, placed into 4% neutral buffered paraformaldehyde and maintained at 4°C until scanning. The skin over the implants was served for the sample orientation. The samples were embedded in agarose gel and imaged using a SkyScan 1172 microCT scanner (Bruker). The 3D micro-CT scans of each Matrigel implant were visualized using Imaris image analysis software (Bitplane). The raw images were 3D

reconstructed, segmented and quantified using Amira 5.5.3 image analysis software (FEI Visualization Sciences Group).

**Ear punch wound healing model**

Eight-week old female CD1 mice (Harlan Laboratories) were used for an ear wounding procedure as described previously[55]. All procedures were carried out according to UK Home Office regulations and under appropriate licences. Briefly, mice were wounded with a 2-mm full-thickness hole punched through the lateral third of each ear using a sterile metal biopsy punch (Harvard Apparatus). The wound was disinfected with ethanol swabs to prevent infection. Mice were daily injected intra-peritoneally with either Tazarotene (10mg/kg body weight) or DMSO 2.6% in PBS (Vehicle) starting from the day of wounding for 6 days. Wounds were photographed with a digital camera immediately after wounding and at day 12. Mice were killed after 12 days or 14 days of wounding, ears were harvested and fixed in 4% neutral buffered paraformaldehyde. A coverslip was laid on top of the ear tissue for flattening. Ear wound images were captured and processed by using stereomicroscope linked to digital camera. Ear hole area (in $mm^2$) was quantified by using ImageJ image analysis software. Tissue from wounded ears was fixed with PFA 4% at 4°C overnight, embedded in paraffin and 7-µm thick sections cut. Before histological staining, slides were dewaxed and rehydrated. Slides were stained with Hematoxylin and Eosin (H&E) or a Picro-Sirius Red stain kit (Sigma). The slides were washed, rehydrated, cleared and mounted. Staining was visualized using Nikon microscope in bright field for Hematoxylin and Eosin (H&E) and under polarized light for Picro-Sirius Red. The Picro-Sirius Red signal was measured in the marginal area of wounds and quantified using Image J software. For labeling of proliferating cells, mice were injected i.p. with 3 mg/kg of EdU (Invitrogen) 24 hours before euthanasia. Ear wound paraffin sections were stained for EdU using Click-iT chemistry following the manufacturer's instructions (Invitrogen). For vascular phenotypic analysis, whole mount preparations of dissected ear skins or paraffin cross-sections were double immunostained. Briefly, after blocking with 5% goat serum in PBST

(0.3% TWEEN-20 in PBS), samples were incubated with anti-mouse CD31 antibody (BD Biosciences). Samples were incubated for with alexa488-conjugated goat anti-rat IgG secondary antibody (Invitrogen) and Cy3-conjugated anti-□-SM actin antibody (Sigma). Nuclei were counterstained with DAPI (Invitrogen). CD31-positive blood vessel area was quantified in the marginal area of wounds using Image J software. Fluorescent images from flat-mounted ear skins were visualized using a Leica SP8 SMD X Confocal Microscope. Around 60 z-stacks of raw images (*xy*) were typically acquired for 3D reconstruction.

**Laser speckle contrast imaging of blood flow**

Blood flow in the ear wounds was monitored using a Speckle Contrast Imager - FLPI-2 (Moor Instruments, UK) as described previously[56]. The FLPI measurements were made in a warm (24 °C) and quiet environment. The CCD camera was positioned 30 cm above the ear internal surface. The contrast images were processed to produce a color-coded live flux image (red denoted high perfusion, blue signified low perfusion) using the moorFLPI-2 measurement module (Moor Instruments). Measurements were made postoperatively in the peripheral area of wounds at 6 and 12 days using the moorFLPI-2 review module (Moor Instruments).



**Excisional dorsal wound healing model**

Eleven-week old female CD1 mice (Harlan Laboratories) were used for cutaneous wounding procedure as described previously[57]. All procedures were carried out according to UK Home Office regulations and under appropriate license. Mice were anesthetized, and their dorsal skin was shaved and wiped with 70% ethanol. Full-thickness excisional wounds were made by picking up a fold of skin and using a sterile, disposable 5-mm biopsy punch, resulting in generation of one wound on each side of the midline. Mice were daily injected intra-peritoneally with either Tazarotene (10mg/kg body weight) or DMSO 2.6% in PBS (Vehicle) starting from the day of wounding for 6 days. The areas of open wounds were measured 0

and 8 days after wounding. Mice were killed after 8 days of wounding, wounds were harvested with a 5-mm rim of unwounded skin tissue and fixed in 4% neutral buffered paraformaldehyde. For immunostaining, paraffin sections were incubated with a rat monoclonal specific for endothelial cells (CD31, BD Bioscience), Cy3-conjugated anti-α-SM actin antibody (Sigma) for smooth muscle cells and myofibroblasts and K14 for keratinocytes (GeneTex). CD31-positive blood vessel area was quantified in the wound edges using Image J software.

**Statistics**

All statistical analysis was carried out using Prism GraphPad. Two treatment groups were compared by unpaired-*t*-test. Multiple group comparisons were analyzed by one-way or two-way ANOVA with *post hoc* Bonferroni's test. A *p* value of less than 0.05 was considered to be statistically significant. Several independent experiments were performed to guarantee reproducibility of findings.



**Acknowledgments.** A.A is supported by the intermediate fellowship awarded by the Oxford British Heart Foundation (BHF) Centre of Research Excellence (RE/08/004/23915). J.E.S is supported by a BHF Senior Basic Science Research Fellowship (FS/11/50/29038). A.C is supported by a BHF Intermediate Basic Science Research Fellowship (FS/11/52/29018). This study was funded by the Oxford BHF Centre of Research Excellence (RE/08/004 and RE/13/1/30181), BHF program grant (RG/11/1/28684), and BHF Chair Award (CH/09/003). The authors acknowledge Wellcome Trust Core Award (090532/Z/09/Z).

**References**


1. Ferrara, N. & Kerbel, R.S. Angiogenesis as a therapeutic target. *Nature* **438**, 967-74 (2005).
2. Adams, R.H. & Alitalo, K. Molecular regulation of angiogenesis and lymphangiogenesis. *Nat Rev Mol Cell Biol* **8**, 464-78 (2007).
3. Potente, M., Gerhardt, H. & Carmeliet, P. Basic and therapeutic aspects of angiogenesis. *Cell* **146**, 873-87 (2011).
4. Henry, T.D. *et al.* The VIVA trial: Vascular endothelial growth factor in Ischemia for Vascular Angiogenesis. *Circulation* **107**, 1359-65 (2003).
5. Barrientos, S., Brem, H., Stojadinovic, O. & Tomic-Canic, M. Clinical application of growth factors and cytokines in wound healing. *Wound Repair Regen* **22**, 569-78 (2014).
6. Loges, S., Roncal, C. & Carmeliet, P. Development of targeted angiogenic medicine. *J Thromb Haemost* **7**, 21-33 (2009).
7. Simons, M. & Ware, J.A. Therapeutic angiogenesis in cardiovascular disease. *Nat Rev Drug Discov* **2**, 863-71 (2003).
8. Al Haj Zen, A. *et al.* Inhibition of delta-like-4-mediated signaling impairs reparative angiogenesis after ischemia. *Circ Res* **107**, 283-93 (2010).
9. Lenard, A. *et al.* In vivo analysis reveals a highly stereotypic morphogenetic pathway of vascular anastomosis. *Dev Cell* **25**, 492-506 (2013).
10. Zanella, F., Lorens, J.B. & Link, W. High content screening: seeing is believing. *Trends Biotechnol* **28**, 237-45 (2010).
11. Arnaoutova, I., George, J., Kleinman, H.K. & Benton, G. The endothelial cell tube formation assay on basement membrane turns 20: state of the science and the art. *Angiogenesis* **12**, 267-74 (2009).

12. Kalluri, R. Basement membranes: structure, assembly and role in tumour angiogenesis. *Nat Rev Cancer* **3**, 422-33 (2003).

13. Arnaoutova, I. & Kleinman, H.K. In vitro angiogenesis: endothelial cell tube formation on gelled basement membrane extract. *Nat Protoc* **5**, 628-35 (2010).

14. Elkins, J.M. *et al.* Comprehensive characterization of the Published Kinase Inhibitor Set. *Nat Biotechnol* **34**, 95-103 (2016).

15. Weindl, G., Roeder, A., Schafer-Korting, M., Schaller, M. & Korting, H.C. Receptor-selective retinoids for psoriasis: focus on tazarotene. *Am J Clin Dermatol* **7**, 85-97 (2006).

16. Sakamoto, K. *et al.* Sensitivity of MLL-rearranged AML cells to all-trans retinoic acid is associated with the level of H3K4me2 in the RARalpha promoter region. *Blood Cancer J* **4**, e205 (2014).

17. Siekmann, A.F. & Lawson, N.D. Notch signalling limits angiogenic cell behaviour in developing zebrafish arteries. *Nature* **445**, 781-4 (2007).

18. Benedito, R. *et al.* Notch-dependent VEGFR3 upregulation allows angiogenesis without VEGF-VEGFR2 signalling. *Nature* **484**, 110-4 (2012).

19. Nagpal, S., Athanikar, J. & Chandraratna, R.A. Separation of transactivation and AP1 antagonism functions of retinoic acid receptor alpha. *J Biol Chem* **270**, 923-7 (1995).

20. Zhao, X., Graves, C., Ames, S.J., Fisher, D.E. & Spanjaard, R.A. Mechanism of regulation and suppression of melanoma invasiveness by novel retinoic acid receptor-gamma target gene carbohydrate sulfotransferase 10. *Cancer Res* **69**, 5218-25 (2009).

21. Chen, J.Y. *et al.* Two distinct actions of retinoid-receptor ligands. *Nature* **382**, 819-22 (1996).

22. Zirn, B. *et al.* All-trans retinoic acid treatment of Wilms tumor cells reverses expression of genes associated with high risk and relapse in vivo. *Oncogene* **24**, 5246-51 (2005).

23. Van Wauwe, J. *et al.* Liarozole, an inhibitor of retinoic acid metabolism, exerts retinoid-mimetic effects in vivo. *J Pharmacol Exp Ther* **261**, 773-9 (1992).

24. Nagpal, S. *et al.* Tazarotene-induced gene 1 (TIG1), a novel retinoic acid receptor-responsive gene in skin. *J Invest Dermatol* **106**, 269-74 (1996).

25. Takami, Y., Yamamoto, I., Tsubouchi, H. & Gohda, E. Modulation of hepatocyte growth factor induction in human skin fibroblasts by retinoic acid. *Biochim Biophys Acta* **1743**, 49-56 (2005).

26. Chen, J.T., Liang, J.B., Chou, C.L., Shyu, R.C. & Lu, D.W. Retinoic acid induces VEGF gene expression in human retinal pigment epithelial cells (ARPE-19). *J Ocul Pharmacol Ther* **21**, 413-9 (2005).

27. Carmeliet, P. *et al.* Synergism between vascular endothelial growth factor and placental growth factor contributes to angiogenesis and plasma extravasation in pathological conditions. *Nat Med* **7**, 575-83 (2001).

28. Inforzato, A. *et al.* The angiogenic inhibitor long pentraxin PTX3 forms an asymmetric octamer with two binding sites for FGF2. *J Biol Chem* **285**, 17681-92 (2010).

29. Brown, N.J., Smyth, E.A., Cross, S.S. & Reed, M.W. Angiogenesis induction and regression in human surgical wounds. *Wound Repair Regen* **10**, 245-51 (2002).

30. Rajnoch, C. *et al.* Regeneration of the ear after wounding in different mouse strains is dependent on the severity of wound trauma. *Dev Dyn* **226**, 388-97 (2003).

31. Metcalfe, A.D., Willis, H., Beare, A. & Ferguson, M.W. Characterizing regeneration in the vertebrate ear. *J Anat* **209**, 439-46 (2006).

32. Buckley, G., Metcalfe, A.D. & Ferguson, M.W. Peripheral nerve regeneration in the MRL/MpJ ear wound model. *J Anat* **218**, 163-72 (2011).

33. Zhang, Y. *et al.* Drug-induced regeneration in adult mice. *Sci Transl Med* **7**, 290ra92 (2015).

34. Clark, L.D., Clark, R.K. & Heber-Katz, E. A new murine model for mammalian wound repair and regeneration. *Clin Immunol Immunopathol* **88**, 35-45 (1998).

35. Pickering, J.G. & Boughner, D.R. Quantitative assessment of the age of fibrotic lesions using polarized light microscopy and digital image analysis. *Am J Pathol* **138**, 1225-31 (1991).

36. Mavria, G. *et al.* ERK-MAPK signaling opposes Rho-kinase to promote endothelial cell survival and sprouting during angiogenesis. *Cancer Cell* **9**, 33-44 (2006).

37. Tammela, T. *et al.* Blocking VEGFR-3 suppresses angiogenic sprouting and vascular network formation. *Nature* **454**, 656-60 (2008).

38. di Masi, A. *et al.* Retinoic acid receptors: from molecular mechanisms to cancer therapy. *Mol Aspects Med* **41**, 1-115 (2015).

39. Gaetano, C. *et al.* Retinoids induce fibroblast growth factor-2 production in endothelial cells via retinoic acid receptor alpha activation and stimulate angiogenesis in vitro and in vivo. *Circ Res* **88**, E38-47 (2001).

40. Cunningham, T.J. & Duester, G. Mechanisms of retinoic acid signalling and its roles in organ and limb development. *Nat Rev Mol Cell Biol* **16**, 110-23 (2015).

41. Shimozono, S., Iimura, T., Kitaguchi, T., Higashijima, S. & Miyawaki, A. Visualization of an endogenous retinoic acid gradient across embryonic development. *Nature* **496**, 363-6 (2013).

42. Duester, G. Retinoic acid synthesis and signaling during early organogenesis. *Cell* **134**, 921-31 (2008).

43. Autiero, M., Luttun, A., Tjwa, M. & Carmeliet, P. Placental growth factor and its receptor, vascular endothelial growth factor receptor-1: novel targets for stimulation of ischemic tissue revascularization and inhibition of angiogenic and inflammatory disorders. *J Thromb Haemost* **1**, 1356-70 (2003).

44. Rusnati, M. *et al.* Selective recognition of fibroblast growth factor-2 by the long pentraxin PTX3 inhibits angiogenesis. *Blood* **104**, 92-9 (2004).

45. Ogawa, A. *et al.* Effect of tazarotene, an acetylenic retinoid, on human dermal fibroblast. *Jpn J Pharmacol* **76**, 317-9 (1998).

46. Rossiter, H. *et al.* Loss of vascular endothelial growth factor a activity in murine epidermal keratinocytes delays wound healing and inhibits tumor formation. *Cancer Res* **64**, 3508-16 (2004).

47. Maden, M. & Hind, M. Retinoic acid, a regeneration-inducing molecule. *Dev Dyn* **226**, 237-44 (2003).

48. Jones, P.H. *et al.* A phase 1 study of tazarotene in adults with advanced cancer. *Br J Cancer* **89**, 808-15 (2003).

49. Falanga, V. Wound healing and its impairment in the diabetic foot. *Lancet* **366**, 1736-43 (2005).

50. Zhang, J.H., Chung, T.D. & Oldenburg, K.R. A Simple Statistical Parameter for Use in Evaluation and Validation of High Throughput Screening Assays. *J Biomol Screen* **4**, 67-73 (1999).

51. Pelz, O., Gilsdorf, M. & Boutros, M. web cellHTS2: a web-application for the analysis of high-throughput screening data. *BMC Bioinformatics* **11**, 185 (2010).

52. Abraham, S. *et al.* A Rac/Cdc42 exchange factor complex promotes formation of lateral filopodia and blood vessel lumen morphogenesis. *Nat Commun* **6**, 7286 (2015).

53. Freeley, M. *et al.* A high-content analysis toolbox permits dissection of diverse signaling pathways for T lymphocyte polarization. *J Biomol Screen* **15**, 541-55 (2010).

54. Lee, S., Barbe, M.F., Scalia, R. & Goldfinger, L.E. Three-dimensional reconstruction of neovasculature in solid tumors and basement membrane matrix using ex vivo X-ray microcomputed tomography. *Microcirculation* **21**, 159-70 (2014).

55. Buckley, G., Wong, J., Metcalfe, A.D. & Ferguson, M.W. Denervation affects regenerative responses in MRL/MpJ and repair in C57BL/6 ear wounds. *J Anat* **220**, 3-12 (2012).

56. Rege, A., Thakor, N.V., Rhie, K. & Pathak, A.P. In vivo laser speckle imaging reveals microvascular remodeling and hemodynamic changes during wound healing angiogenesis. *Angiogenesis* **15**, 87-98 (2012).

57. Canesso, M.C. *et al.* Skin wound healing is accelerated and scarless in the absence of commensal microbiota. *J Immunol* **193**, 5171-80 (2014).

58. Perlman, Z.E. *et al*. Multidimensional drug profiling by automated microscopy. *Science* **306**, 1194-8 (2004).

**Figure Legends**

**Figure 1** Phenotypic screen for angiogenic activity of LOPAC$^{1280}$ small molecule library. **a)** *Left:* Screening workflow. Primary Human Umbilical Vein Endothelial Cells (HUVEC) were seeded onto Matrigel coated 384-well plates and incubated with LOPAC$^{1280}$ compounds at a concentration of 10 μM. *Right:* Plate design. The position of negative controls (Vehicle (DMSO) alone, blue), positive controls (Suramin, 10μM, red) and LOPAC$^{1280}$ small molecules (green) is indicated. **b)** Image analysis workflow: *Top:* Endothelial tubes were stained for F-actin using phalloidin and CellMask Green and then imaged using an Operetta high content microcopy system. The region of interest (ROI, middle panel) is created on 16-bit red channel images and is followed by automated image segmentation (bottom panel) to identify tubes (white mask), nodes (green), and branching points (red dots) using Metamorph image analysis software (Molecular Devices). Scale bar 1 mm. **c)** *Left:* Scatter-plot distribution showing the results of high content screening. The total tube length was normalized using the B-score method in WebCellHTS2. Inhibitors and enhancers (B-Score ≤-4 and ≥+2.6 respectively) are indicated below and above the orange lines. Negative controls (are shown in blue positive controls in red and LOPAC$^{1280}$ library molecules in green. *Right,* Representative microscopic images from negative (Vehicle alone) and positive (Suramin) control wells, Scale bar 400 μm.



**Figure 2** Validation of active lead compounds. **a)** Selected enhancer hits were re-tested manually using the endothelial tube formation assay in 96-well format. The tubes were imaged and quantified as described in Figure 1. *Left*: Representative images of active lead compounds at 10μM. Scale bar 500μm. *Right,* the chemical structure, the molecular weight, the primary target of the compound and its effect on the total tube length (normalized to Vehicle %100), n=3 each concentration. Data are expressed as mean±s.e.m, one-way ANOVA followed by Bonferroni's *post hoc* test, **p<0.01; ***p<0.001 compared to Vehicle. **b)** The effect of active lead compounds was tested in an organotypic angiogenesis assay

where HUVECs are plated on to a confluent human dermal fibroblast (HDF) layer. The medium containing the compound (7μM) was refreshed at 3 and 5 days following plating of endothelial cells. Co-cultures were stained with an antibody against CD31 and imaged 7 days after endothelial cell plating. Nine fields were quantified for each well (n=6 wells per group). Error bars, mean±s.e.m, one-way ANOVA followed by Bonferroni's *post hoc* test, *p<0.05; ***p<0.001 compared to Vehicle. Scale bar 1mm. **c)** Dose-response curve showing the effect of Tazarotene on total tube length using the organotypic angiogenesis assay. Data are shown as mean±s.e.m. The curve was fitted using Prism GraphPad, and $EC_{50}$ calculated as 0.8μM. Scale bar 200 μm. **d)** High-power image of Vehicle and tazarotene treated endothelial tubes, demonstrating lateral filopodia protrusions (arrows). Scale bar 50 μm **e)** Effect of Tazarotene (3 μM) on expression of FLT4 (VEGFR3) and KDR (VEGFR2) in cultured endothelial cells estimated using RT-qPCR. Error bars, mean±s.e.m., *P=0.02 compared to Vehicle, (n=3 replicates derived from 3 independent experiments, analysed using unpaired *t*-test).



**Figure 3** Tazarotene induces angiogenesis through RAR activation. HUVEC were seeded on to confluent human dermal fibroblast (HDF) cells. Medium containing the compound (3 μM) was refreshed 3 days following plating of endothelial cells. Co-cultures were stained with anti-CD31 and imaged 5 days after endothelial cell plating. Angiogenic phenotype parameters (total tube length, branching points, tube thickness, and total node area) of the formed network were measured using Metamorph image analysis software. Nine fields were quantified for each well as described in the methods. **a)** Effect of natural retinoic acids (all-*trans*-retinoic acid (ATRA) and 9-*cis*-retinoic acid), RAR isoform agonists (RARα (BMS753), RARβ (CD2314) and RARγ(BMS961)) and RXR agonist (SR 11237) on angiogenic phenotype, compared to the Tazarotene-induced phenotype (n=3 wells per condition). Error bars, mean±s.e.m, one-way ANOVA followed by Bonferroni's *post hoc* test, **p<0.01; ***p<0.001 compared to Vehicle. Scale bar 200 μm. *Right*, Heatmap of z-score scaled data from the four angiogenic parameters, followed by hierarchical clustering of compounds to create the dendrogram

generated by Spotfire software[58]. Compounds clustering together, exhibit similar phenotypic profiles[58]. **b)** Effect of the pan-RXR antagonist (UVI 3003), pan-RAR antagonist (BMS5493) and Tazarotene on angiogenic phenotype (n=3 wells per conditions). Error bars, mean±s.e.m, one-way ANOVA followed by Bonferroni's *post hoc* test, ***p<0.001. Scale bar 200 μm. *Right*, compound phenotypic profiling using hierarchical cluster analysis as described above. **c)** Effect of Liarozole (3 μM), a retinoic acid metabolism inhibitor, on angiogenic phenotype, n=6 wells per conditions. Data are expressed as mean±s.e.m. Unpaired-*t*-test, **p<0.01; ***p<0.001 compared to Vehicle. Scale bar 200μm. **d)** RARRES1 mRNA abundance in Tazarotene-treated HUVEC and HDF assessed by quantitative RT-PCR (n=3 replicates derived from 3 independent experiments). Unpaired-*t*-test, **p<0.01 compared to Vehicle.



**Figure 4** Tazarotene enhances the pro-angiogenic paracrine effects of fibroblasts. **a)** *Left*, representative images showing the effect of Tazarotene (7 μM) on cell number and DNA synthesis in isolated HUVECs. HUVEC were cultured as single cells in presence of Tazarotene or Vehicle for 48 hours. EdU (10μM) was added 6 hours before fixation. Cells were stained for EdU (green) and DAPI (blue). Scale bar 200μm. **b)** *Left*, representative images showing the effect of Tazarotene (7 μM) on cell number and DNA synthesis in HUVEC/HDF co-culture at presence of Tazarotene or Vehicle for 48 hours. Cells were stained for EdU (green) and CD31 (red). Scale bar 200μm. Right panels of **a)** and **b)**, quantitative data for total cell number and the proportion of EdU positive nuclei. Cell counts and EdU positive cells were normalised to the Vehicle control, which was set at 100%. Data from 4 wells for each concentration, and nine fields per well were analysed, and are expressed as mean±s.e.m. One-way ANOVA followed by Bonferroni's post hoc test, *p<0.05; **p<0.01; ***p<0.001 compared to Vehicle. **c)** Effect of 5μM , representative images showing the effect of Tazarotene ted secreted proteins from HDF cells using Proteome Profiler Array™. The inset shows the raw images from the array membrane for Vehicle (top) and Tazarotene (below), with letters corresponding to those on the bar-graph.

Fluorescence intensity of each dot was normalized to the Vehicle control and presented as fold change (y-axis) on the bar graph. d) Effect of 3 μM Tazarotene PGF and PTX3 mRNA expression estimated by quantitative RT-PCR. Error bars, mean±s.e.m. n=3. Unpaired-*t*-test, **p<0.01 compared to Vehicle. **(e)** Effect of Tazarotene on secreted PGF and PTX3 assayed by ELISA. n=3 per treatment condition, error bars, mean±s.e.m. One-way ANOVA followed by Bonferroni's *post hoc* test, *p<0.05; **p<0.01; ***p<0.001 compared to Vehicle.

**Figure 5 Tazarotene promotes functional neovascularization in Matrigel implants**. Mice were injected subcutaneously with Matrigel supplemented with FGF-2 (250 ng/ml). Tazarotene (10 mg/kg) or Vehicle (DMSO) was injected intra-peritoneally (i.p.) daily for 6 days. **a)** Representative photographs of implants from Vehicle control and Tazarotene treated mice. **b)** Effect of Tazarotene on neovessel formation. *Top:* Histological sections of Matrigel implants double immunostained for CD31 (endothelial marker, green) and α-smooth muscle actin (α-SM actin, smooth muscle cell marker, red). The dotted line shows the edge of Matrigel implant. Scale bar 120μm. *Bottom*: Mature neovessel area (y-axis) in the Matrigel plug was quantified by measuring CD31-positive neovessel invested by α- smooth muscle actin–positive cells stained areas in three sections (with a 1-mm interval between sections) for each implant and divided by total implant area, n=6 animals per treatment group, 2 implants per animal were studied. Data are presented as box plots, with maximum, minimum, and quartile range. Two-way ANOVA (****p<0.0001) followed by Bonferroni's multiple comparisons test, *p<0.05, ***$p$<0.001 compared to Vehicle group. **c)** Effect of Tazarotene on microvessel perfusion using microCT angiography. *Top*, microCT angiogram of Matrigel implants. Mice were infused with Microfil 12 days after Matrigel implantation and the harvested implant analysed by 3D microCT imaging to visualize the microvasculature (orange). *Middle:* 3D-reconstruction of microCT images of Matrigel implants including the perfused microvessels: vessels inside Matrigel (green), vessels surrounding Matrigel (red) and the Matrigel implant (transparent grey). *Bottom:* The vessel volume inside the Matrigel was

quantified using Amira image analysis software. Data are expressed as % (vessel volume/Matrigel implant volume) by box plots, with maximum, minimum, and quartile range, n=6 mice, 2 implants per treatment group. Unpaired-*t*-test, *p<0.05 compared to Vehicle group. Scale bar 2mm. **d)** Effect of Tazarotene on microvessel perfusion using confocal microscopy. Representative Z-stack confocal images of thick sections of Matrigel implants (n=3 mice, 2 implants per treatment). To visualize vessel perfusion, terminally anaesthetised mice were injected with biotinylated IsolectinB4 12 days after implantation, implants harvested and sections immunolabeled for CD31 (green, endothelial cells), α-SM actin (red, smooth muscle cells), DAPI (Blue, Nuclei), and for injected lectin by using streptavidin-Alexa 647 (purple, perfused vessels). The dotted line shows the edge of Matrigel implant. Scale bar 120μm.

**Figure 6 Tazarotene promotes ear punch wound healing and neovascularization after injury. a)** Effect of Tazarotene on ear punch closure. *Left:* Representative images of ears from mice treated with Vehicle or Tazarotene. Tazarotene (10 mg/kg, i.p.) was administered daily for 6 days following the ear-punch. Wound size was measured after 12 days. *Right:* Quantification of the punch area (n=6 animals per group). Data are presented as box plots, with maximum, minimum, and quartile range, unpaired-t-test, ***p<0.001 compared to Vehicle group. **b)** *Left:* Effect of Tazarotene on blood flow following ear-punch injury. Representative images showing blood flow measured in the wound area using speckle contrast laser imaging at 6 and 12 days after injury (n=5 animals per group). The dotted circle denotes the region-of-interest. *Right*: Mean flow (flux) in the region-of interest was quantified using moorFLPI-2 software, and data expressed as mean ± s.e.m. Two-way ANOVA (**p<0.01) followed by Bonferroni's multiple comparisons test, *p<0.05 compared to Vehicle. **c)** Effect of Tazarotene on wound histology at 14 days after injury. *Left:* Hematoxylin and eosin stained cross-sections with the 2-mm area of the original hole indicated. Arrows indicate the initial wound site identified by the cartilage cut. *Middle:* Enlargement of the boxed section in the previous panel. Arrow-heads indicate new hair follicles

in the wound bed. *Right*: Picrosirius red stained cross-sections. Birefringence of picrosirius differentiates thick, mature collagen fibers (red/yellow) from thin, new collagen (green). Quantification of collagen density, data expressed as % (stained collagen area/regenerated area), n=6 animals per group. Unpaired-*t*-test, *p<0.05 compared to Vehicle. Dotted line shows the initial cut position. Scale bar 90μm. **d)** Effect of Tazarotene on cell proliferation in the wound area. *Left:* Representative confocal images of ear wound at 6 days after injury stained with *upper panel*, CD31 (green), α-SM actin (red), DAPI (blue) and EdU (white); *lower panel*, stained with EdU (green), Keratin 14 "K14" (red) and DAPI (blue). The arrow indicates the initial wound site. Scale bar 90 μm. *Right:* EdU positive cells were quantified and normalized to the total cell number inside the regenerated area which is identified by the cartilage cut, n=4 animals per treatment condition. Data are expressed as mean±s.e.m. Unpaired-t-test, ***p<0.001 compared to vehicle group. **e)** Effect of Tazarotene on wound neovascularization at 14 days after injury. *Left:* Cross sections of ear punches were stained with CD31 (green), α-SM actin (red) and DAPI (nuclei). Arrows indicate the initial wound site. Scale bar 90 μm. *Right:* CD31-positive microvessel area was quantified as a percentage of the regenerated area, n=6 animals per group. Unpaired-*t*-test, ***p<0.001 compared to Vehicle group. **f, g)** Effect of Tazarotene on new vessel formation in the regenerating zone. Z-stack confocal images of flat mounted ears at day 4 **(f)** and day 14 **(g)** after injury. The dotted line indicates the wound site, the arrows shows new hair follicles, and the asterisk indicates the ear hole. CD31 (green, endothelium) and □-SM actin (red, smooth muscle cell and myofibroblasts). Insets in **(g)** show a global view of the wound at low magnification. Scale bar 90 μm.

**Figure 7. Tazarotene enhances excisional dorsal wound healing and wound bed vascularization. a)** Effect of Tazarotene on wound closure. *Left*: Representative images of skin from mice treated with Vehicle or Tazarotene. Scale bar 5mm *Right*: Quantification of the wound closure (n=6 animals per group). Data are presented as box plots, with maximum, minimum, and quartile range, unpaired-t-test, *p<0.05 compared to Vehicle group. **b)** Effect of Tazarotene on wound epithialization. *Left:*

Haematoxylin and eosin stained cross-sections of wound centre. Scale bar 500 μM Arrows indicate the wound edges. *Middle*: Enlargement of the boxed section in the previous panel. Arrow-heads indicate new hair follicles in the wound bed. Scale bar 500 μM *Right*: Cross sections of wound centre were stained with Keratin 14 (green), α-SM actin (red) and DAPI (nuclei). Arrows indicate the initial wound site. Scale bar 90 μm. **c)** Effect of Tazarotene on new vessel formation in wound bed. *Left*, Cross sections of wounds were stained with CD31 (green), α-SM actin (red) and DAPI (nuclei). Scale bar 50 μm. *Right:* CD31-positive microvessel area was quantified as a percentage of the wound bed area, n=6 animals per group. Arrows indicate the wound edges. Unpaired-*t*-test, *$p<0.05$ compared to Vehicle group.

**Fig 1**

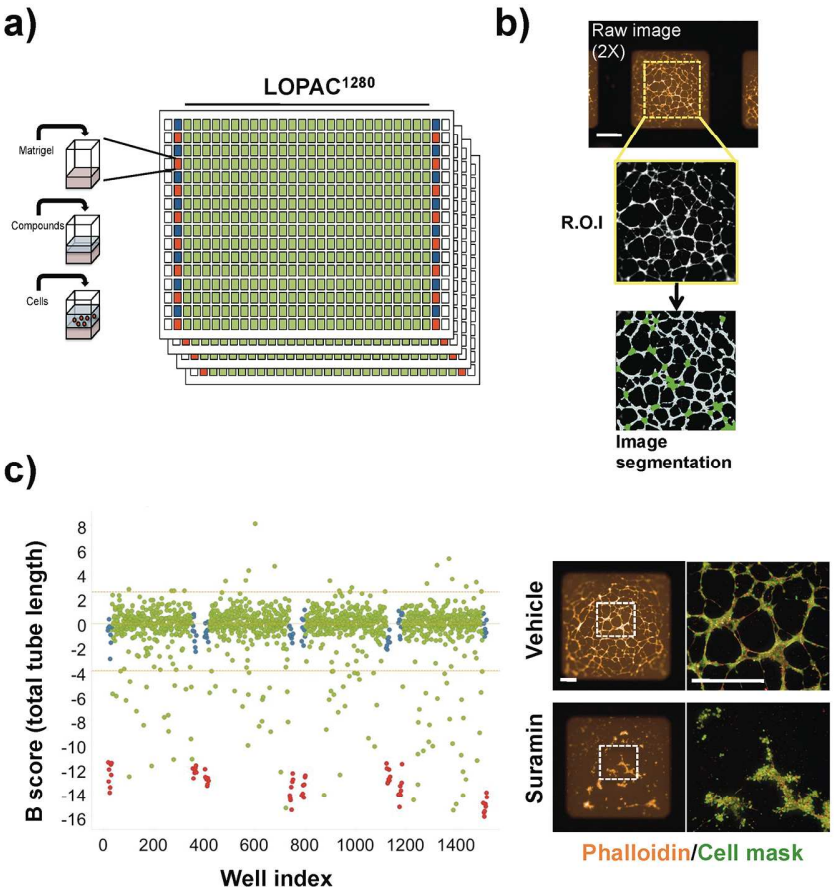

Fig 2

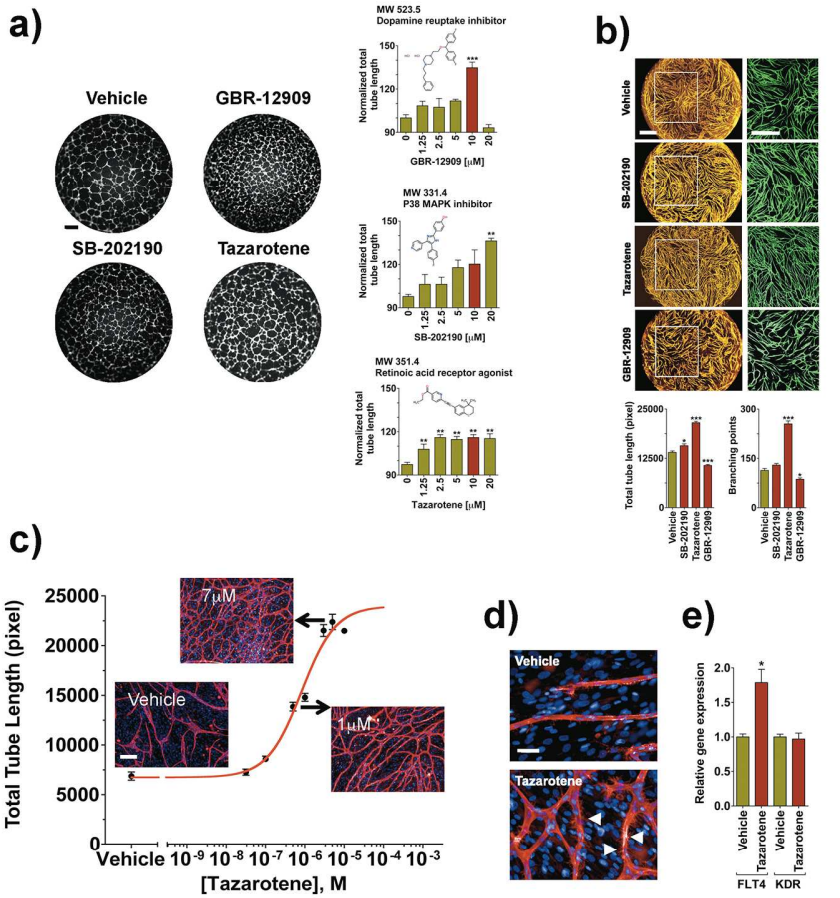

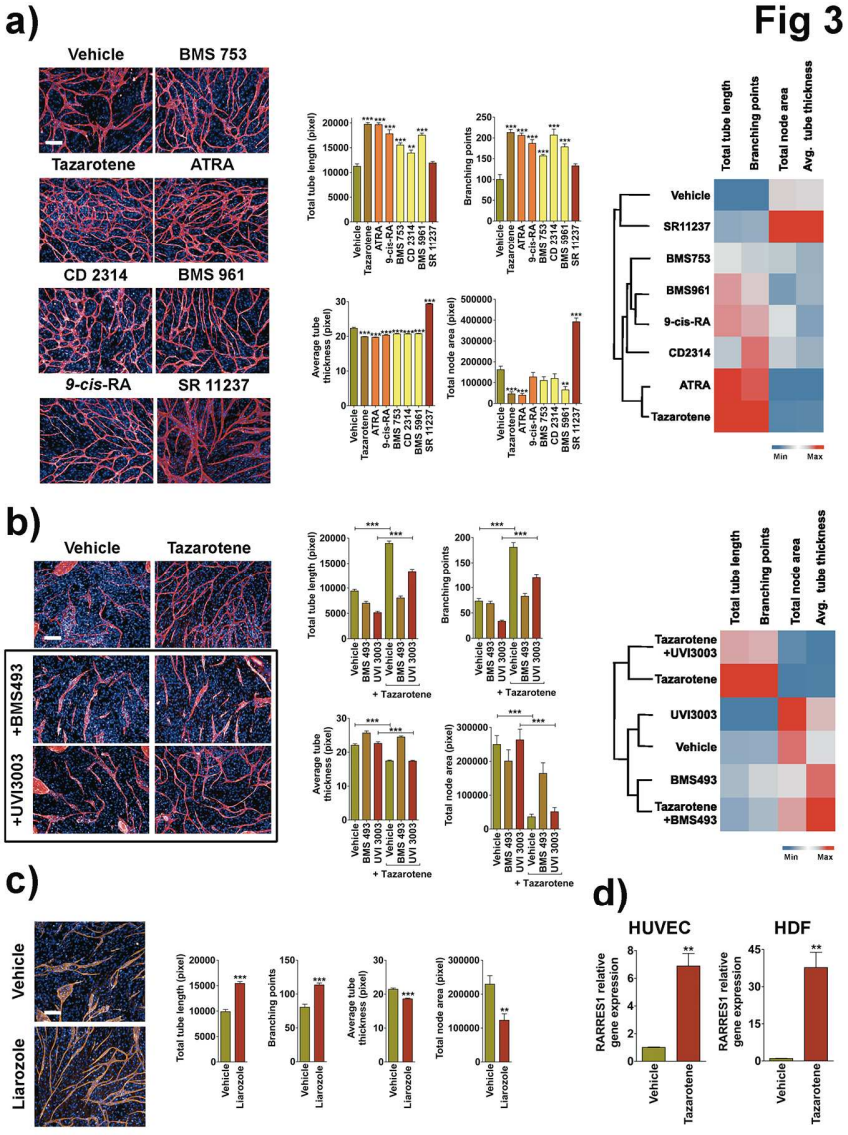

Fig 4

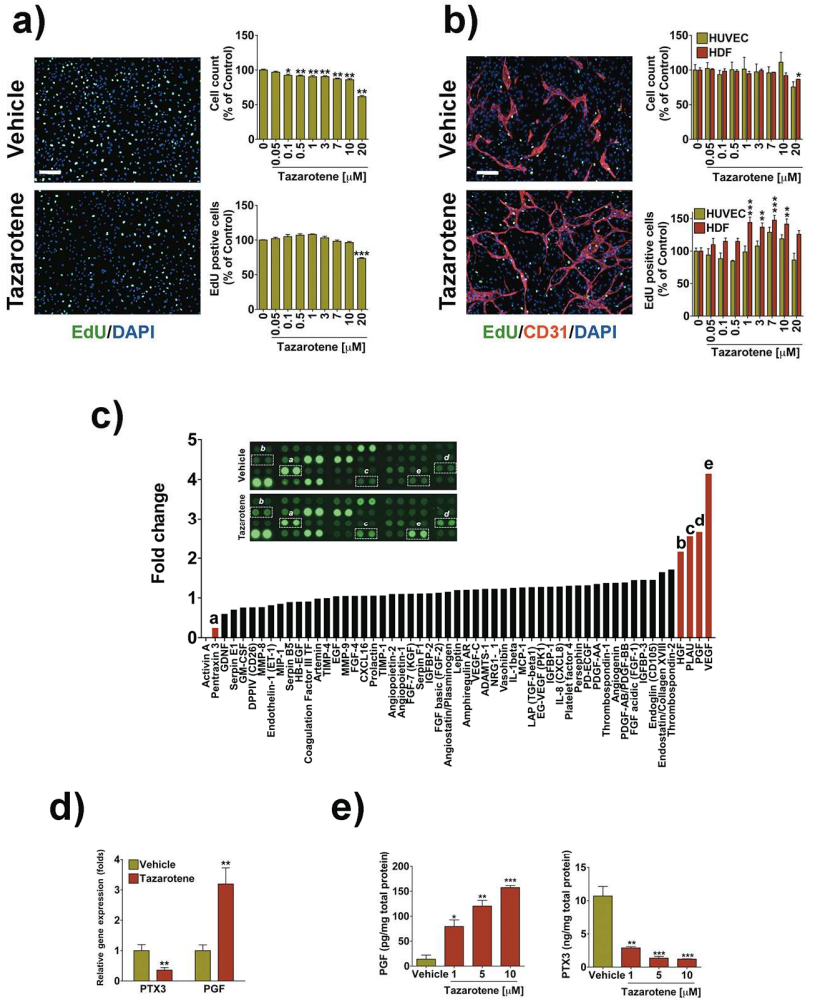

Fig 5

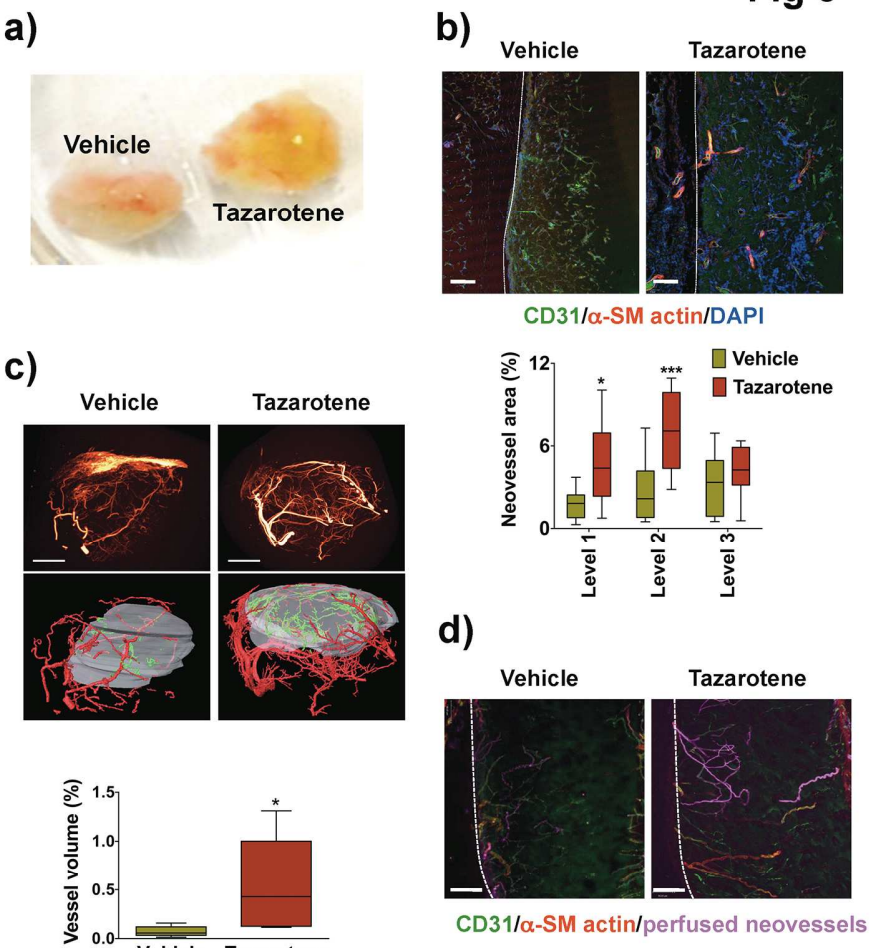

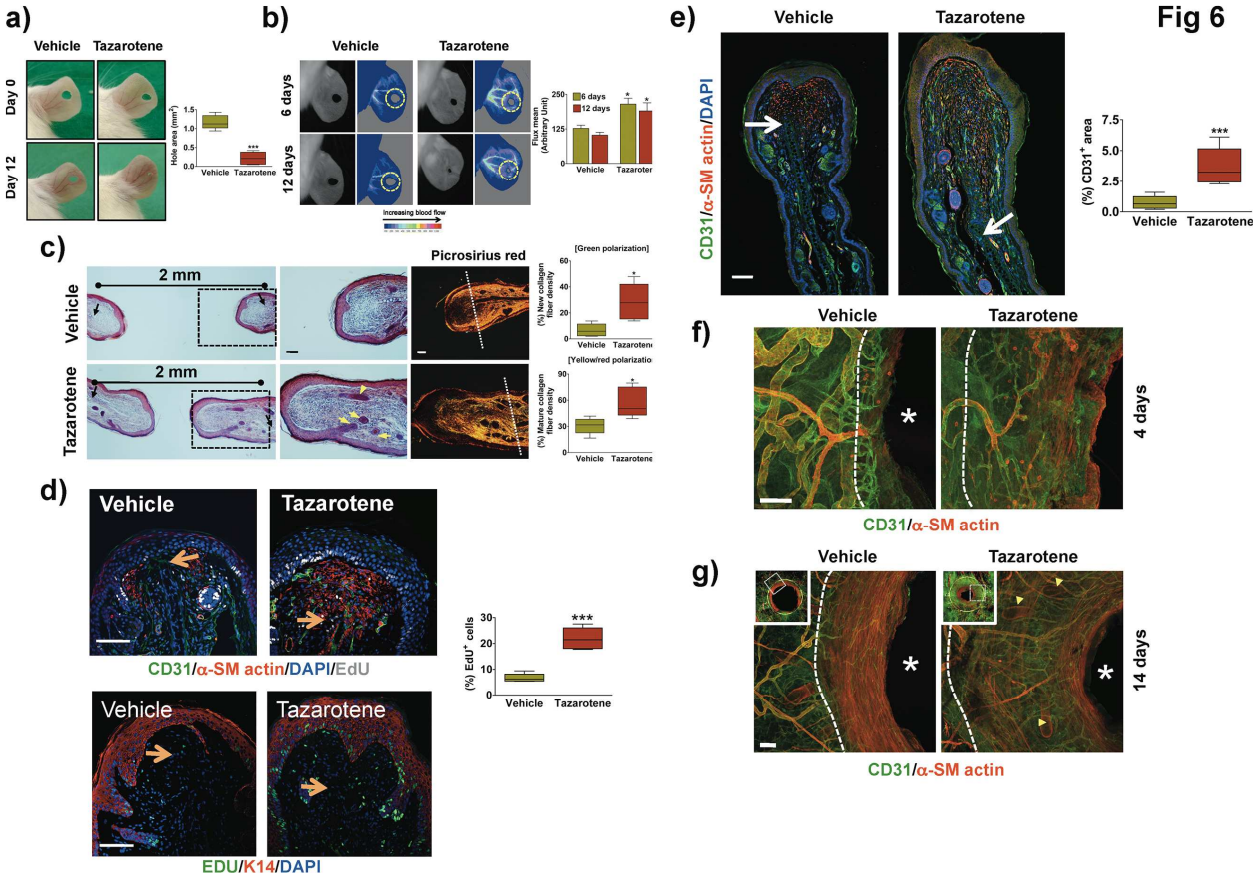


Fig 6

Fig 7